BIOCHEMISTRY

Computation-driven redesign of an NRPS-like carboxylic acid reductase improves activity and selectivity

Kun Shi[1]†, Ju-Mou Li[1]†, Mu-Qiang Wang[1], Yi-Ke Zhang[1], Zhi-Jun Zhang[1], Qi Chen[1], Frank Hollmann[2], Jian-He Xu[1], Hui-Lei Yu[1]*

Engineering nonribosomal peptide synthetases (NRPSs) has been a "holy grail" in synthetic biology due to their modular nature and limited understanding of catalytic mechanisms. Here, we reported a computational redesign of the "gate-keeper" adenylation domain of the model NRPS-like enzyme carboxylic acid reductases (CARs) by using approximate mechanism-based geometric criteria and the Rosetta energy score. Notably, *Mab*CAR3 mutants ACA-1 and ACA-4 displayed a remarkable improvement in catalytic efficiency (k_{cat}/K_M) for 6-aminocaproic acid, up to 101-fold. Furthermore, G418K exhibited an 86-fold enhancement in substrate specificity for adipic acid compared to 6-aminocaproic acid. Our work provides not only promising biocatalysts for nylon monomer biosynthesis but also a strategy for efficient NRPSs engineering.

INTRODUCTION

Nonribosomal peptide synthetases (NRPSs) are crucial enzyme machineries to synthesize pharmacologically valuable natural products, such as penicillin, bleomycin, and cyclosporine (*1*). These megaenzymes, often hundreds of kilodaltons in size, consist of multiple modules, each comprising at least three domains: the adenylation (A) domain, the thiolation (T) domain, and the condensation (C) domain (Fig. 1A) (*2*, *3*). Their modular architecture offers the vast combinatorial design space, which has sparked the interest of synthetic biologists to engineer NRPSs to obtain tailored peptides with different bioactivities (*4*–*7*). Despite major advances in understanding NRPS enzymology, success engineering is still rare due to the complex molecular interactions among modules and domains, necessitating an insight of protein-protein interactions and substrate specificities (*8*–*10*).

Structural and biochemical evidence indicates that the substrate-activating A domain acts as the first "gate keeper," substantially influencing substrate specificity (*9*, *11*–*16*). The key Lys residue (A10 Lys) forms hydrogen bonds with the carboxyl group in the substrate and the oxygen atoms in the ribose moiety of adenosine 5′-triphosphate (ATP) to gather them in the A domain binding pocket (*13*, *17*). The substrate carboxyl group then undergoes nucleophilic attack by the α-phosphorus atom of ATP, forming the pentacoordinated transition state (Fig. 1C) (*1*, *17*). At last, acyl–adenosine 5′-monophosphate (AMP) complex and inorganic pyrophosphate (PPi) are released through cleavage of the P—O bond. In light of that, researchers have been developing different approaches to engineer the substrate specificity of A domains, such as domain swapping, directed evolution, and structure-based semi-rational design (*4*). However, existing high-throughput screening techniques exhibit limited universality and must undergo customized refinement and optimization for distinct substrates or products, thereby reducing engineering efficiency.

In recent years, physics-based virtual screening has become effective methods for obtaining target enzyme mutants (*18*). In a pioneering study, Chen *et al.* (*19*) reported a computational redesign of the A domain of NRPS gramicidin S synthetase A using their self-developed K* algorithm. The top-scored mutants were expected to have a lower K_M for the target substrate. However, enzyme design cannot overlook the importance of catalytic efficiency, which hinges on a deeper understanding of the high-energy transition states. Calculating quantum mechanical (QM) descriptors is often computationally expensive and involves a sophisticated workflow encompassing conformer generation, geometry optimization, and ultimately a single-point density functional theory calculation for each molecule. This limitation restricts the applicability to extensive enzyme virtual screening. Thus, faster approximation methods, such as the near-attack conformation (NAC) strategy, have been developed to describe the transition state trend (*20*). For example, the CASCO protocol, rooted in the NAC strategy, used Rosetta Design in combination with molecular dynamics (MD) simulations for predicting highly stereoselective enzyme mutants (*21*, *22*).

NRPS-like proteins, such as carboxylic acid reductases (CARs), catalyze the reduction of carboxylic acids to aldehydes in the presence of ATP and reduced form of nicotinamide adenine dinucleotide phosphate ($NADP^+$) (NADPH) (*11*). Owing to their broad substrate specificity, CARs demonstrate remarkable potential as key enzymes in the metabolic toolbox for the biosynthesis of polymer precursors, biofuels, flavors, and fragrances (*23*–*29*). CARs were considered a more suitable model system for A domain engineering, thanks to their single module (Fig. 1B) and compact size (~120 kDa), which enables easier genetic manipulation, expression in heterologous hosts, and protein purification (*30*). In general, native CARs have been shown to have little to no activity on amino acids, which is different from NRPS (*31*). Recently, we found a CAR, *Mab*CAR3, which exhibited potential for the biosynthesis of 6-aminocaproic acid (6-ACA) and 1,6-hexamethylenediamine (HMD), key monomers to nylon production (Fig. 2) (*32*). However, the limited natural activity of *Mab*CAR3 toward adipic acid (AA) and 6-ACA hindered the propulsion of the cascade reaction toward the ultimate HMD. On

[1]State Key Laboratory of Bioreactor Engineering, School of Biotechnology, East China University of Science and Technology, 130 Meilong Road, Shanghai 200237, People's Republic of China. [2]Department of Biotechnology Institution, Delft University of Technology, Van der Maasweg 9, 2629HZ Delft, Netherlands.
*Corresponding author. Email: huileiyu@ecust.edu.cn
†These authors contributed equally to this work.

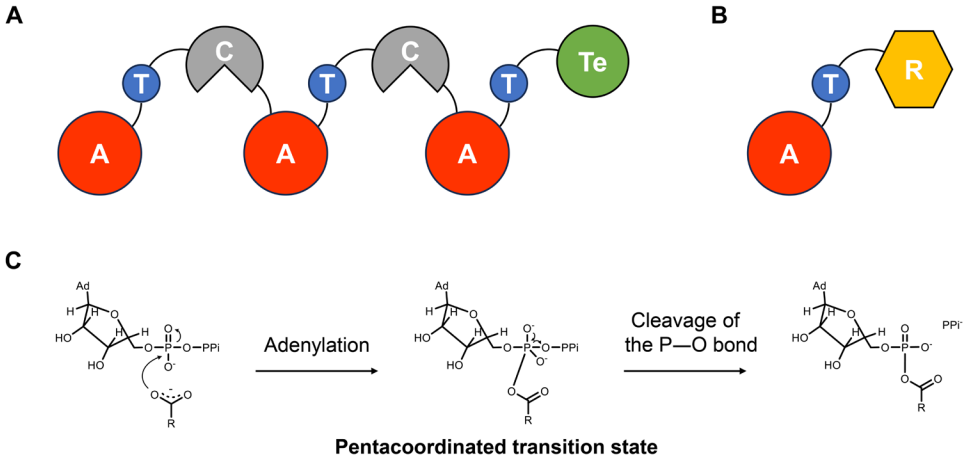

Fig. 1. General domain organization of NRPSs and NRPS-like protein CARs and their adenylation mechanism. (**A**) Domain arrangement of typical NRPSs. (**B**) Domain architecture of NRPS-like protein CARs. (**C**) Proposed mechanism in the adenylation reactions. A, adenylation domain; T, thiolation domain; C, condensation domain; Te, thioesterase domain; R, reductase domain.

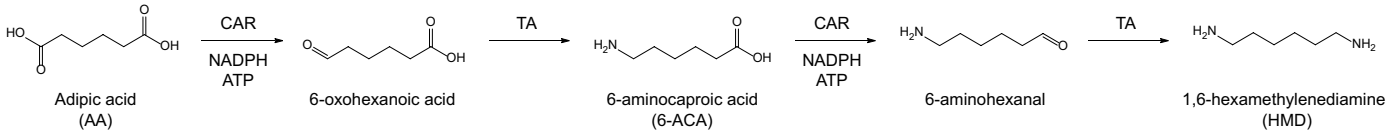

Fig. 2. Enzymatic routes toward the synthesis of 6-ACA and HMD from AA. CAR, carboxylic acid reductase; TA, transaminase.

the other hand, the suboptimal substrate specificity between α,ω-diacids and ω-amino fatty acids (e.g., $U_{AA}/U_{6\text{-}ACA}$), which led to the generation of unwanted byproduct 6-aminohexanal from a fraction of ω-amino fatty acids, contributed to the diminished yield of ω-amino fatty acids.

Here, we computationally optimized the active site environment for target substrates by using approximate mechanism-based geometric criteria and the Rosetta energy score, obviating the need for more expensive MD simulations. The *Mab*CAR3 enzyme was efficiently engineered to generate a series of tailored enzymes with enhanced activity and substrate selectivity. As a result, we achieved the highest biosynthesis productivity of key nylon monomers (such as 6-ACA and HMD) reported to date.

RESULTS

Computational redesign of *Mab*CAR3

Previous studies have elucidated the proposed adenylation mechanism through a combination of x-ray crystallography (*11*, *33*), site-directed mutagenesis (*11*, *23*, *33*–*35*), and MD calculations (*17*). ATP binds to the center of the *Mab*CAR3 A domain, establishing many molecular contacts that are conserved across the ANL (acyl-CoA synthetases, NRPS adenylation domains, and Luciferase enzymes) superfamily (*13*, *17*). K618 should monitor the negative charge on the initial complex, stabilize the pentacoordinated transition state, and release PPi before forming the AMP-substrate complex (*17*). The carboxylate substrate-binding pocket is lined with hydrophobic residues, and conserved H301 and T422 are near the ATP α-phosphate and the substrate carboxylate group that probably involved in catalytic processes (Fig. 3) (*11*).

However, to our knowledge, the details of the pentacoordinated transition state in CARs remain elusive, as no theoretical studies using QM calculations have been performed. Fortunately, hybrid QM/molecular mechanical (QM/MM) simulations have been performed with the pentacoordinated transition state in other adenylating enzymes (*36*–*40*), which could help us roughly understand this step in CARs. In our recent study, we approximated the NAC geometry of the adenylation step, which holds notable potential for the virtual screening of CAR k_{cat} (*32*). Here, we further optimized the geometric constraints of enzyme-substrate interactions and extended to *Mab*CAR3 redesign (Fig. 3).

We postulated that substrate specificity could be adjusted by altering interactions with new substituent groups in the target substrate and reshaping the hydrophobic binding pocket to further optimize the protein-ligand interaction network. Therefore, a scan was conducted for residues within 5 Å of the substrate and those within 6 Å that had side chains oriented toward the substrate. After excluding the residues that participated in ATP binding and performed a conserved catalytic role in the process, a total of 10 residues (L284, A303, L306, L342, V344, G393, G395, G418, G420, and G426) were targeted for redesign (Fig. 3).

Furthermore, we derived insights from the research by Black *et al.* (*41*), in which the Rosetta energy score (interface_dE) was designated as the binding affinity score between the substrate and the active site, facilitating the virtual screening for K_M determination. Consequently, this approach enabled a preliminary in silico prediction of the enzyme performance (k_{cat}/K_M) toward specific substrate by predicting k_{cat} and K_M separately (Fig. 4). A limited set of designs was chosen for experimental characterization with guidance by the parameters Rosetta energy score (interface_dE) and NAC frequency, aiming to increase the anticipated activity or substrate selectivity.

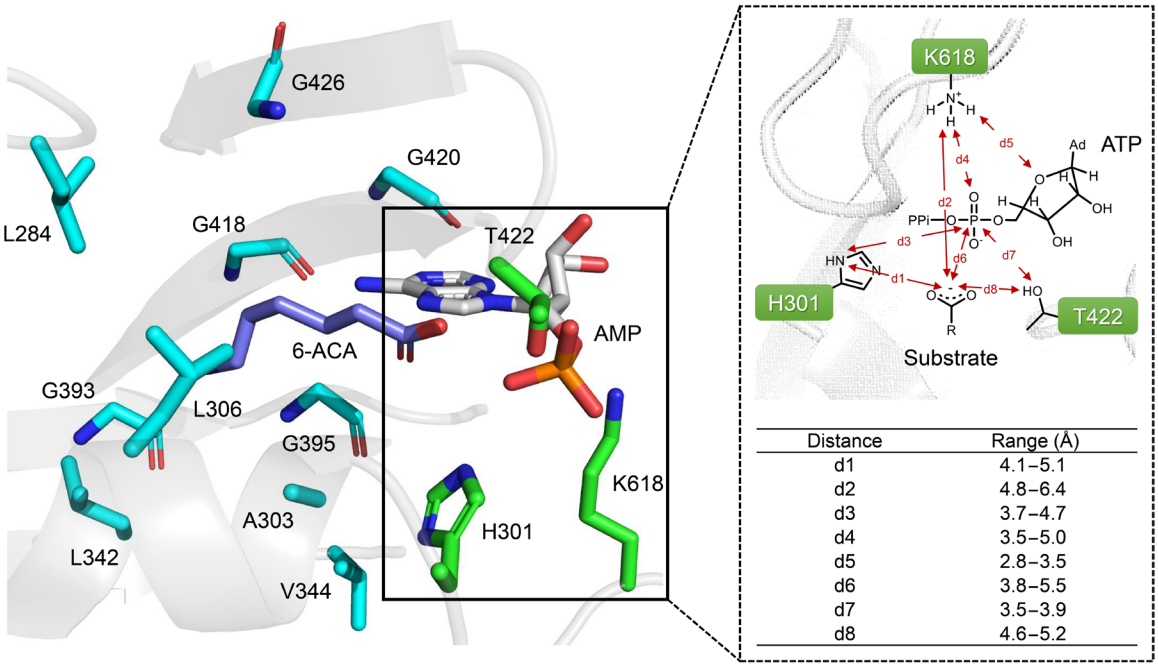

Fig. 3. Key residues and NAC criteria in the A domain pocket of *Mab*CAR3. Light blue denotes residues selected for design. 6-ACA, 6-aminocaproic acid. Green denotes conservative residues involved in catalytic process. The structure of adenylation domain was constructed using AlphaFold2, and the 6-ACA conformation was generated using the Schrödinger Maestro conformational search module.

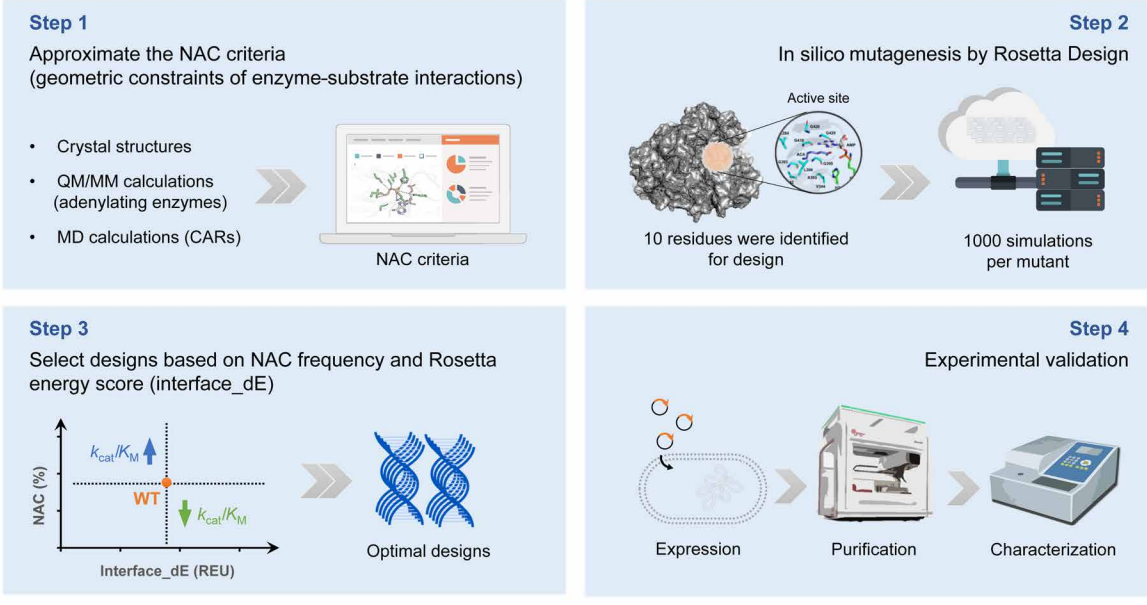

Fig. 4. Schematic representation for the computational redesign of *Mab*CAR3. Step 1: Establish the approximate NAC criteria. Step 2: In silico mutagenesis of the 10 key residues by Rosetta Design. Step 3: Selection of designs based on the NAC frequency and Rosetta energy score. Step 4: Expression, purification, and characterization of the designs. QM, quantum mechanical; MM, molecular mechanical.

Design of *Mab*CAR3 for enhanced activity toward ω-amino fatty acids

The first target product was aliphatic α,ω-diamines, such as HMD, which is used as a nylon 66 monomer. The aim of this approach was to increase the activity toward 6-ACA or even surpass that toward AA, thereby driving the entire cascade toward the synthesis of HMD and decrease the accumulation of the intermediate 6-ACA. However, because of computational power limitation, calculating all possible combinations of the selected 10 residues is nearly impossible.

The mutability landscape approach is a powerful tool in enzyme directed evolution (*42*). A multitude of protein variants were scrutinized to elucidate the impact of each single amino acid substitution

on enzyme activity, selectivity, or stability. This approach provides intricate knowledge on the connections between sequence and function, helping designers make informed choices about protein sequence space and substantially minimizing screening effort (*43*). Thus, we introduced an in silico mutability landscape-guided strategy to mitigate the computational workload associated with virtual screening of multisite combinatorial mutations.

In the first step, in silico site saturation mutagenesis was performed on the 10 residues in the pocket, using 6-ACA as the substrate. A total of 38 designs were selected for activity testing using the wild-type enzyme as a reference (fig. S1A and table S1). As a result, 95% of the mutations were positive (61%) or neutral (34%) (fig. S2), affirming the robustness of the virtual screening methodology and providing a foundation for the creation of a combinatorial mutation library (table S2).

Next, 18 candidates with greater NAC frequency and lower interface_dE (Fig. 5A and table S3) were chosen for characterization from approximately 8000 designs after in silico multisite mutagenesis. A total of 17 mutants were successfully constructed (ACA-16 with no soluble expression), and 15 enzymes exhibited a more than fivefold increase in activity toward 6-ACA (Fig. 5B). Of these, ACA-4 exhibited the most notable increase in activity toward 6-ACA, with a specific activity of 1.1 U/mg. Moreover, initial success was achieved in altering the substrate preference of CAR from AA to 6-ACA ($U_{6\text{-ACA}}/U_{AA} = 2.5$), underscoring its advantageous role in our HMD synthesis cascade (Fig. 5C).

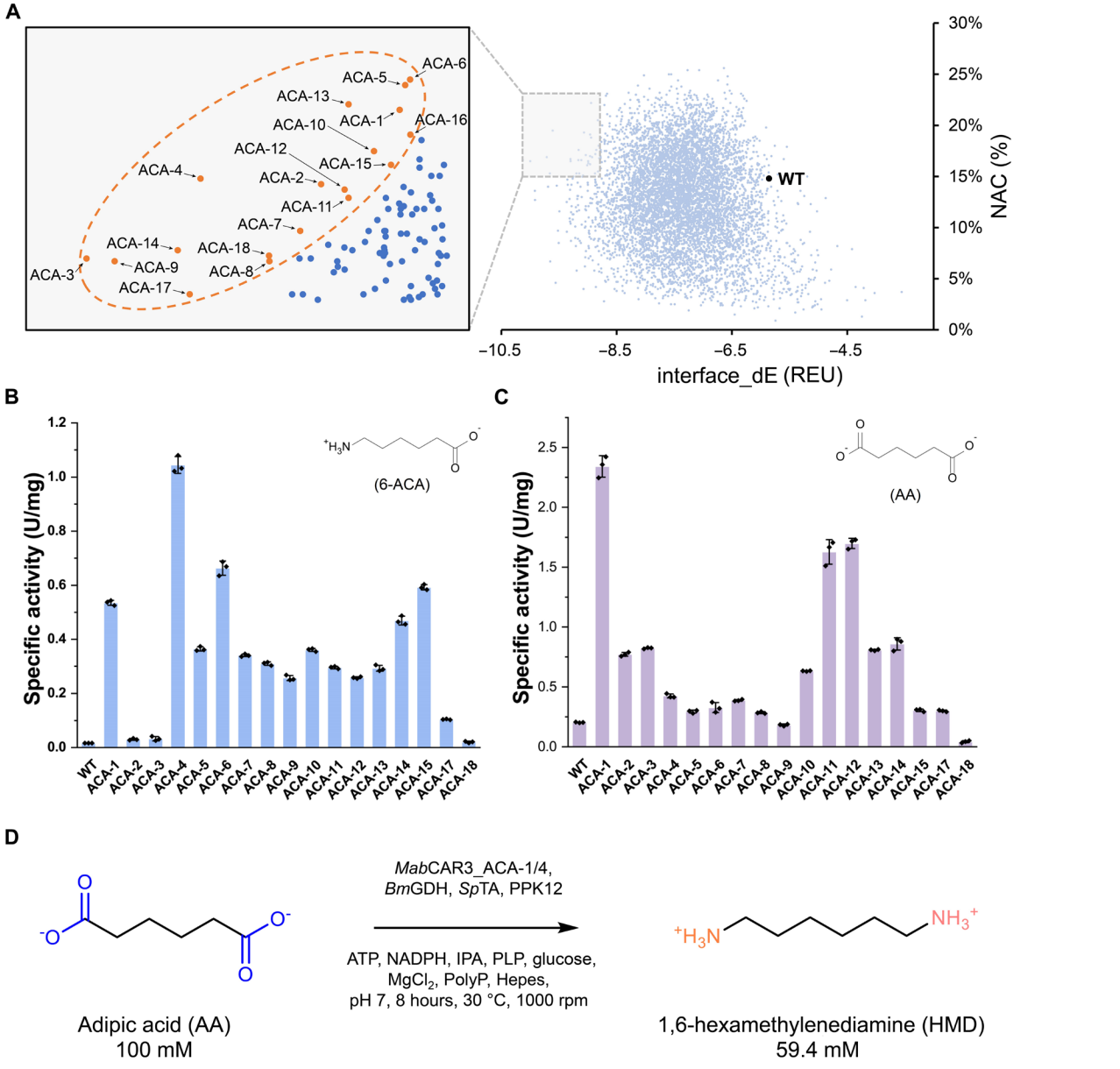

Fig. 5. Computational redesign of *Mab*CAR3 for HMD biosynthesis. (**A**) In silico multi-site mutagenesis (6-ACA as substrate). Orange points: 18 mutations selected for experiment characterization (table S3). (**B**) Deamination activity of the 17 designs toward 6-ACA. (**C**) Deamination activity of the 17 designs toward AA. Data [in (B) and (C)] are presented as mean values ± SD ($n = 3$ independent experiments). (**D**) Conversion of AA to HMD using purified ACA-1, ACA-4, and other necessary enzymes.

Rosetta modeling analysis revealed that the four mutations (L284I, L306M, L342E, and G393E) in ACA-4 optimized the native hydrophobic interaction network and facilitated the formation of salt bridges between the substrate's ω-amino group and the surrounding residues (fig. S3). Another mutant, ACA-1 (L284D/A303M/L306I/L342E/G393A), significantly improved the activity toward 6-ACA ($P < 0.05$) and increased the activity toward AA by 11-fold, reaching the highest known value thus far (2.3 U/mg) (Fig. 5C). Kinetic analysis of ACA-1 revealed a 101-fold increase in k_{cat}/K_M toward 6-ACA compared to the wild-type enzyme (Table 1). The substrate affinity of ACA-1 toward 6-ACA was significantly enhanced by approximately 11-fold ($P < 0.05$), with K_M reduced to 7.0 mM, representing the best value reported to date. ACA-1 had catalytic properties complementary to those of ACA-4, implying its potential for synergistic utilization in cascade reactions.

We next explored whether the substrate scope of the best designs (ACA-1 and ACA-4) could be extended toward other aliphatic α,ω-diacids and ω-amino acids with varying carbon numbers, encompassing more than 90% of the nylon monomer market. Similar to previous reports on other bacterial CARs (*32*, *44*), the activities of ACA-1 and ACA-4 increased as the substrate's carbon chain was elongated (Fig. 6). Compared to ACA-1, ACA-4 displayed a more pronounced increase in activity toward most ω-amino fatty acids (C5 to C10) rather than toward α,ω-diacids (table S4). Intriguingly, both designs showed peak activity enhancement toward 6-ACA, providing additional evidence for the targeted specificity achieved through computational design.

Biosynthesis of HMD with mutants ACA-1 or/and ACA-4

First, we attempted in vitro biotransformation with purified enzymes. Our preliminary experiments revealed that ACA-4 significantly outperformed other variants ($P < 0.05$), increasing HMD yield 17-fold compared to the wild type (WT) (table S5). Subsequently, using 100 mM 6-ACA as a substrate, purified ACA-4, ω-transaminase *Sp*TA, and other essential enzymes demonstrated 82.5% yield to HMD (fig. S4). Furthermore, the ACA-1 + ACA-4 cascade produced 59.4 mM HMD in 8 hours with 100 mM AA as substrate, achieving the highest reported productivity (0.86 g liter^{-1} hour^{-1}) (Fig. 5D), reaching a level that matched the highest reported value for the de novo biosynthesis of AA [0.81 g liter^{-1} hour^{-1}; (*45*)] (Table 2). The 6-ACA (7.2 mM) and a minor quantity of AA (<1 mM) were identified in the reaction system, indicating the presence of approximately 33 mM aldehyde intermediates (6-oxohexanoic acid and 6-aminohexanal). This implied that the rate-limiting step in this cascade shifted from carboxylic acid reduction to aldehyde amination. Further efforts are needed to enhance the activity of ω-transaminase.

We extended the reaction scale to a larger system (10 ml) for the conversion of AA to HMD. Turner's group observed that using crude enzymes in a similar CAR-transaminase multienzyme system did not lead to a substantial overall reduction in yield, with less than 6% aldehyde being overreduced by endogenous alcohol dehydrogenases from *Escherichia coli* (*46*). Hence, we used condensed crude enzymes in this cascade reaction to reduce purification costs. As depicted in fig. S5, the highest HMD yield of 53.0% was achieved from 50 mM AA in 24 hours, yielding none of the undesired alcohols as a side product. Furthermore, high-purity HMD was isolated (4.5 mg, 98.0% purity; fig. S6).

Tailoring the substrate selectivity for the synthesis of 6-ACA

The next target was aliphatic ω-amino acids, which included 6-ACA, the monomer of nylon 6. In our recent work, we found that strict substrate selectivity was crucial for enhancing the yield of 6-ACA because 6-ACA could be further reduced to the corresponding aldehyde (*32*, *47*). We aimed to develop a tailored design for *Mab*CAR3 with improved activity toward AA while decreased activity toward 6-ACA, thereby enhancing its potential for the synthesis of ω-amino fatty acids.

In silico site saturation mutagenesis (AA as substrate) was also conducted (fig. S1B). After comparing the results with those of previous in silico mutagenesis studies of 6-ACA, we selected 16 designs based on the NAC frequency and Rosetta energy score for experimental characterization (Fig. 7A and table S6). The best design, G418K, demonstrated a fivefold increase in activity toward AA compared with WT and a fivefold decrease in activity toward 6-ACA compared with WT, resulting in a 397-fold difference between the specific activities toward these two substrates (1065 mU/mg toward AA versus 3 mU/mg toward 6-ACA) (Fig. 7B and fig. S7). Kinetic analysis was well consistent with the trend observed in the in silico mutagenesis results, with higher K_M and lower k_{cat} for 6-ACA and lower K_M and higher k_{cat} for AA (86-fold enhanced $\frac{k_{cat}/K_M(AA)}{k_{cat}/K_M(6-ACA)}$; Table 1).

The enzyme-substrate binding model revealed that new salt bridges [N(418 K)-COOH(AA)] and hydrophobic interactions [CB(418 K)-C6(AA)] were formed between the carboxyl group of G418K and the substrate AA (fig. S8, A and C) (*48*). Simultaneously, hydrophobic interactions between the enzyme and central regions of AA were intensified, such as CB(A303)-C2(AA) and CD1(L306)-C3(AA). As depicted in fig. S8 (B and D), modeling revealed that native hydrophobic interactions between G418K and 6-ACA were

Table 1. Kinetic profiles of *Mab*CAR3-WT and its best designs toward AA and 6-ACA.

	AA			6-ACA		
CAR	**k_{cat} (s^{-1})**	**K_M (mM)**	**k_{cat}/K_M (M^{-1} s^{-1})**	**k_{cat} (s^{-1})**	**K_M (mM)**	**k_{cat}/K_M (M^{-1} s^{-1})**
WT	1.53 ± 0.15	42.2 ± 17.2	36.4 ± 8.90	0.29 ± 0.06	78.5 ± 28.4	3.60 ± 1.10
G418K	2.65 ± 0.38	5.11 ± 0.86	518 ± 43.8	0.10 ± 0.03	176 ± 12.0	0.60 ± 0.29
ACA-1	6.28 ± 0.90	7.21 ± 1.71	870 ± 52.9	2.63 ± 0.29	7.24 ± 2.24	363 ± 32.6
ACA-4	1.01 ± 0.11	4.77 ± 1.02	212 ± 11.0	6.95 ± 2.26	22.2 ± 8.59	313 ± 43.9

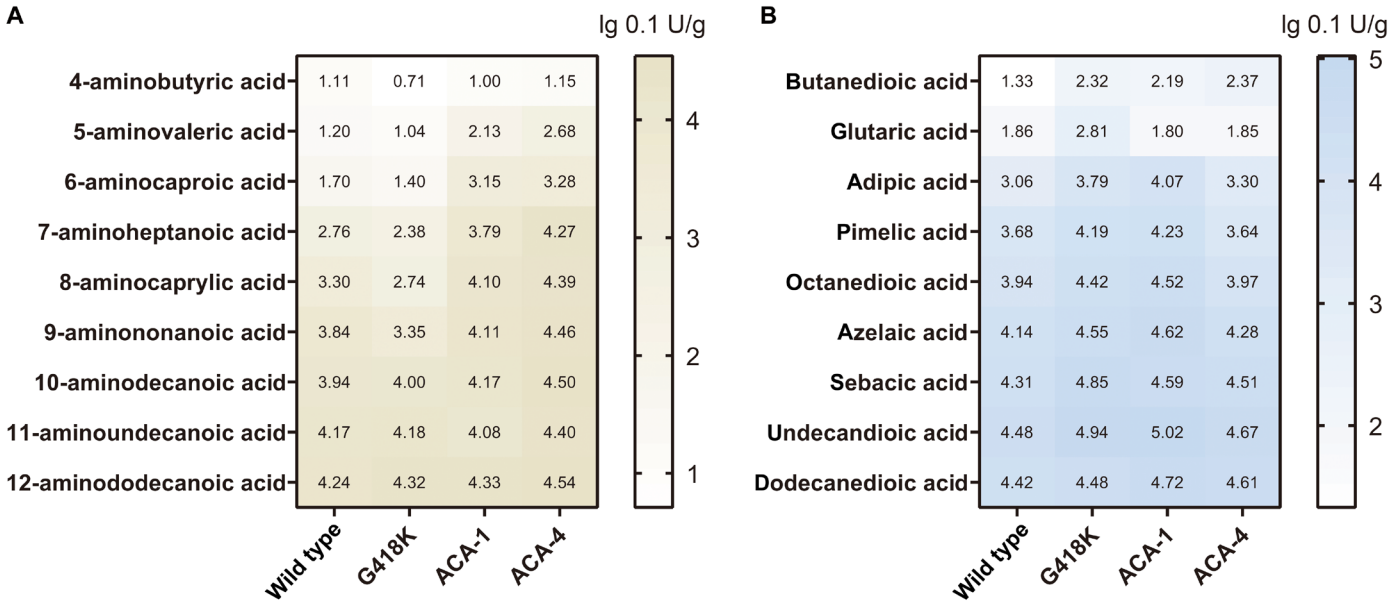

Fig. 6. The heatmap represented CAR activities with various ω-amino fatty acids and α,ω-diacids. (**A**) ω-amino fatty acids as substrates. (**B**) α,ω-diacids as substrates. Data were shown as logarithmic (lg 0.1 U/g). Assays were conducted with 5 mM substrate.

Table 2. Comparison for HMD biosynthesis. ADH, alcohol dehydrogenase; CHMO, Baeyer-Villiger cyclohexanone monooxygenase; Lact, lactonase; CAR, carboxylic acid reductase; AKR, aldo-keto reductase; ω-TA, ω-transaminase; Cyp, cytochrome P450 monooxygenase. N/A, not describe in the paper.

Substrate		Catalyst	Titer (mM)	Productivity (g liter^{-1} hour^{-1})
Petroleum-based	Cyclohexanol	ADH, CHMO, Lact, CAR, AKR, and ω-TA	16.6	0.088 (*56*)
	Cyclohexanol	ADH, CHMO, Lact, CAR, AKR, and ω-TA	4.2	N/A (*57*)
	Cyclohexane	Cyp, ADH, CHMO, Lact, CAR, AKR, and ω-TA	7.6	0.040 (*56*)
Bio-based	AA	CAR (MAB4714 and MAB4714_L342E) and ω-TA	3.0	0.046* (*33*)
	AA	CAR (*Mab*CAR3) and ω-TA	1.0	0.005 (*32*)
	AA	CAR (MAB4714 and MAB4714_L342E) and ω-TA	2.1	0.010 (*58*)
	AA	CAR (*Mab*CAR3_L342D) and ω-TA	11.2	0.072 (*47*)
	AA	CAR (*Mab*CAR3_ACA-4 and ACA-1) and ω-TA	59.4	0.863 (this work)
	6-ACA	CAR (*Mab*CAR3_ACA-4) and ω-TA	82.5	1.599 (this work)

*The production time recorded in the original text was "overnight," which was calculated as 8 hours here.

disrupted. For instance, the distance between CD2 (L342) and C4 (6-ACA) increased from 3.9 to 6.3 Å, and the distance between CB (A303) and C2 (6-ACA) increased from 4.3 to 4.8 Å. These interaction changes could be the primary reasons for the increase in $U_{AA}/U_{6\text{-}ACA}$.

Next, we explored the activity of G418K toward more α,ω-diacids and ω-amino fatty acids with varying carbon chain lengths (C4-C12) (Fig. 6). Compared to the WT, the mutants exhibited higher $U_{\alpha,\omega\text{-diacids}}/U_{\omega\text{-amino fatty acids}}$ (by 3- to 24-folds) except for the C12 substrate, and their activity toward α,ω-diacids increased (2.5- to 10-folds) (fig. S9).

Purified G418K and other enzymes were employed in the synthesis of 6-ACA. After 6 hours, the 6-ACA concentration reached 87.5 mM (Fig. 7C), affording a production rate of 1.91 g liter^{-1} hour^{-1} (Table 3). Subsequent large-scale reactions (10 ml) with condensed crude enzymes giving the ω-amino fatty acids (C6 to C9) in good yield (49 to 74%), achieving the highest reported product concentrations in the literature and demonstrating considerable potential for

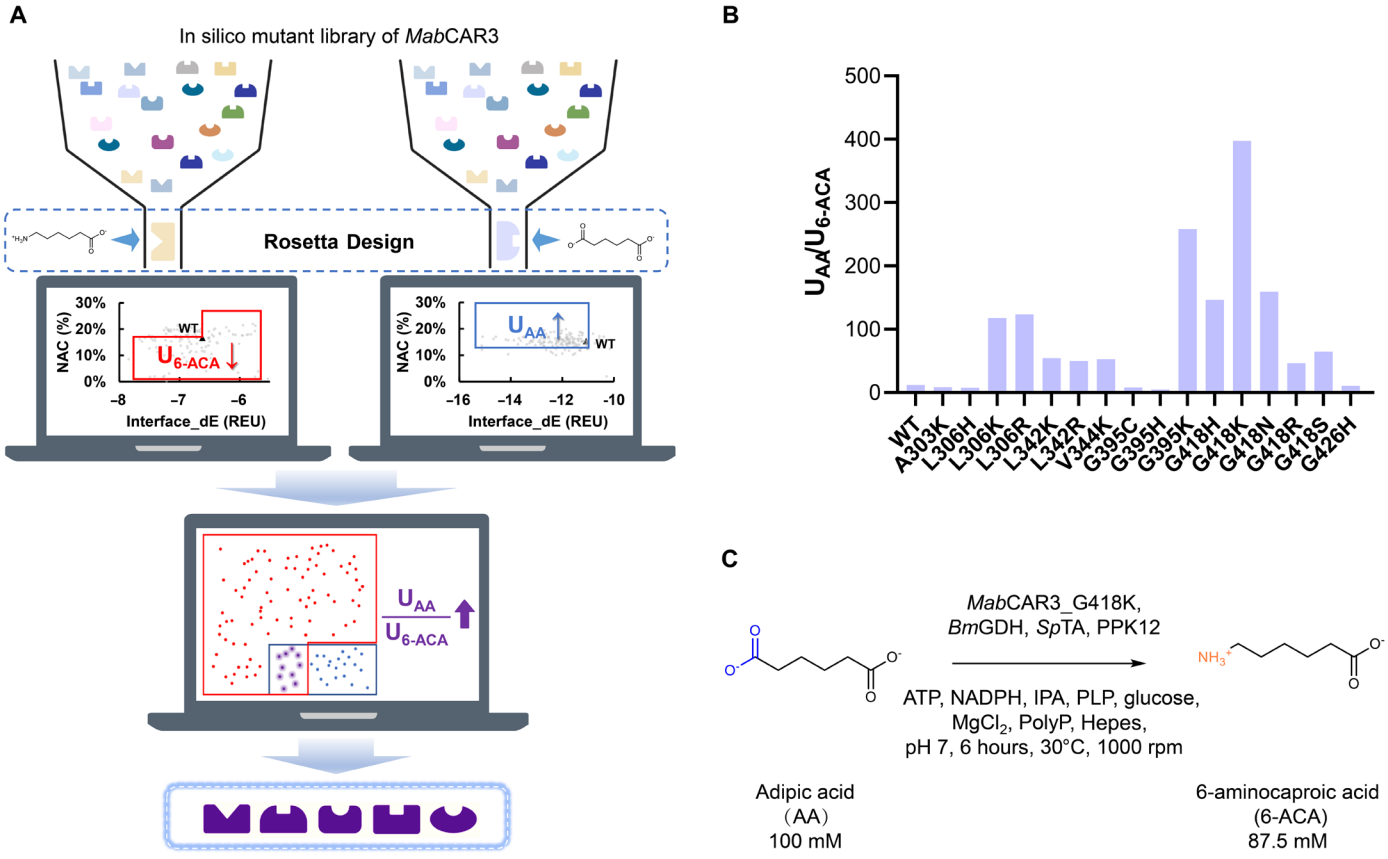

Fig. 7. Computational redesign of *Mab*CAR3 for 6-ACA biosynthesis. (**A**) Sixteen designs were selected on the basis of in silico site mutagenesis toward AA and 6-ACA. (**B**) $U_{AA}/U_{6\text{-}ACA}$ of the 16 designs and WT. Detailed activity toward 6-ACA and AA were shown in fig. S7. (**C**) Conversion of AA to 6-ACA using purified *Mab*CAR3_G418K and other necessary enzymes.

Table 3. Comparison for 6-ACA biosynthesis. BVMO, Baeyer-Villiger cyclohexanone monooxygenase; AHR, aldehyde reductase; CDH, cyclohexanol dehydrogenase; NifV, homocitrate synthase; AksD/E/F, 3-isopropylmalate dehydratase; KdcA, branched-chain alpha-ketoacid decarboxylase; Vfl, pyruvate transaminase; KivD, α-ketoisovalerate decarboxylase.

Substrate		Catalyst	Titer (mM)	Productivity (g liter^{-1} hour^{-1})
Petroleum-based	Cyclohexanol	ADH, BVMO, Lact, ω-TA, and AHR	97	0.268 (*59*)
	Cyclohexylamine	BVMO, Lact, AHR, and ω-TA	48	0.262 (*60*)
	Cyclohexane	Cyp, CDH, CHMO, Lact, ADH, and ω-TA	8.6	0.282 (*61*)
Bio-based	Glucose	NifV, AksD/E/F, KdcA, Vfl, KivD, and ω-TA	0.26	<0.001 (*62*)
	AA	CAR (MAB4714) and ω-TA	8.8	0.144* (*33*)
	AA	CAR (*Ki*CAR) and ω-TA	4.5	0.033 (*32*)
	AA	CAR (*Ki*CAR_G299K) and ω-TA	7.6	0.055 (*47*)
	AA	CAR (*Mab*CAR3_G418K) and ω-TA	87.5	1.912 (this work)

*The production time recorded in the original text was overnight, which was calculated as 8 hours here.

application (fig. S10). The formation of alcohol byproducts (such as 6-hydroxyhexanoic acid and 1,6-hexanediol) was not detected in the reaction.

Furthermore, the preparative biotransformation experiment was performed in a 0.5-liter reactor (0.4-liter reaction mixture) with 50 mM substrate AA (fig. S11). Through derivatization with Boc_2O, purification by silica gel column chromatography, and concentration by rotary evaporation, a high-purity 6-ACA derivative was isolated (2.13 g, >92.3% purity; fig. S12) with a yield of 46.0%. The generated biocatalyst effectively converted AA into 6-ACA at a gram scale, a substantial step toward scalable bioproduction.

DISCUSSION

Similar to typical NRPS, several studies have shown that the substrate specificity of CAR can be modified by the mutation of the active-site residues in A domain (*23*, *33*–*35*). However, these A domain engineering efforts depend on customized high-throughput screening methods and/or structure-guided small mutant libraries. For example, Kramer *et al.* (*34*) used a growth-coupled selection method and achieved a 17-fold improvement in catalytic efficiency, which is the highest reported increment to date in CAR engineering. However, this pales in comparison to the hundredfold improvements seen in other intensively studied enzymes, such as transaminases (*49*, *50*). Our initial endeavor involved constructing an amino benzamidoxime–based screening method for 6-oxohexanoic acid/6-aminohexanal, intermediate products in this work, ended in failure, despite amino benzamidoxime being a classic aldehyde derivatization reagent (*35*). Therefore, we turned to computational enzyme design, offering cost-effective exploration of numerous candidate mutations with greater versatility and reproducibility than traditional experimental approaches (*18*).

Computational enzyme design must rely on simplified models that approximate real protein-ligand interactions, especially in the high-energy transition states (*19*). While accurate QM calculations can provide valuable insights into enzyme catalysis, rapid exploration of a larger sequence space is more crucial for enzyme design. Designers must balance model accuracy against computational resources. Our work showed that the approximate NACs, obtained through fitting, can be used to expand the physical model–based computational design from a specific enzyme-substrate system with QM data to a group of enzyme-substrate systems that share the same catalytic mechanism, which produced results akin to classical QM-based works. In addtion, the in silico mutant library was screened on the basis of the penalty score of the NAC geometric constraints and the protein-ligand affinity score using Rosetta Design, similar to the strategy recently proposed by Yang *et al.* (*49*). Rosetta Design uses a Monte Carlo search algorithm, which has a lower computational cost compared to MD simulations, and can be parallelized using multiple cores for high-throughput virtual screening (*50*). Here, we used 6 Intel Xeon Platinum 8370 processors, achieving a virtual screening rate of 1000 enzyme mutants per day. By simplifying both high-energy transition state modeling and conformational search, we provided a cheap and versatile design approach for reasearcher with limited computational resources.

With relatively little and high-efficiency experimental effort, 72 mutants were screened and tested to identify the optimal designs (with a 70% positive rate) (Figs. 5 and 7). Without a requirement for further optimization by laboratory evolution, these redesigned enzymes exhibited excellent catalytic activity and/or substrate specificity toward the target substrates, substantially enhancing the conversion efficiency and progressing toward high substrate loading and high yield production. Notably, the increase in biotransformation productivity from AA to 6-ACA/HMD (>0.86 g $liter^{-1}$ $hour^{-1}$) reached a level that matched the highest reported value for the de novo biosynthesis of AA (0.81 g $liter^{-1}$ $hour^{-1}$) (*45*), aligning effectively with industrial demands.

In addition, the redesigned enzymes successfully afforded a wide range of nylon monomers with varying carbon chain lengths (C6 to C12), which was a further advantage. Enzyme catalysis has limited success in synthesizing bulky chemicals, such as nylon. Biobased nylon 56 is the only successful product, as more than 90% of the nylon monomers are chemically synthesized from petroleum-based sources. The enhanced activity and selectivity of the CARs demonstrated the potential for producing most of the nylon monomers available on the market, including nylon 6, nylon 66, nylon 11, nylon 12, nylon 46, nylon 610, nylon 612, and nylon 1010 (Fig. 6).

Notwithstanding the broad success of A domain substrate specificity engineering, we do not suggest that A domain engineering in isolation can unlock the full potential of these megaenzymes. To further enhance HMD/6-ACA production from AA, we recommend combining beneficial mutations in the T and R domains, as well as thermostability engineering, which has been proven to be an effective strategy (*51*, *52*).

In summary, our findings indicated that combining the approximate NAC geometry and Rosetta Design is effective at predicting suitable CAR designs with high activity and/or specificity, facilitating the tailored biosynthesis of nylon monomers without the need for specialized QM simulations or high-throughput screening methods. Our engineering strategies can inspire the development of other NRPSs as computational algorithms continue to improve.

MATERIALS AND METHODS

Computational protein redesign

A model of *Mab*CAR3's adenylation domain was constructed using AlphaFold2 (*53*), and an ensemble of substrate conformations (AA or 6-ACA) was generated using the Schrödinger Maestro conformational search module. Key binding pocket residues were identified through published MD calculations (*17*) and crystal structures with bound substrates (Protein Data Bank: 6OZ1, 5MSD, and 5MST) (*11*, *33*). Substrate geometry constraints corresponding to NACs were derived from MD calculations in the adenylation domain of CARs, QM/MM calculations of the pentacoordinated transition state in other adenylating enzymes (*36*–*39*), and the crystal structure with the protein-ligand interface (*11*, *33*). Rosetta Design with default settings was used for computational redesign. The .xml files, Flags files, .cst files, and submit.sh files used for Rosetta Design were modified from previous works by Siegel's group (*41*) and Meiler's group (*54*). Variants were screened based on NAC frequency and the Rosetta energy score (interface_dE), with threshold values set depending on the WT (*32*). Experimental validations were performed on selected candidates.

Plasmid construction and protein purification

Plasmids used in this work were listed in table S7 and transformed into *E. coli* BL21 (DE3). Gene synthesis services were provided by

GenScript (Nanjing) and Tsingke (Shanghai) in this work. The CAR variants were constructed using the ClonExpress MultiS One Step Cloning Kit (Vazyme), and the incorporation of mutations was confirmed by DNA sequencing from Tsingke (Shanghai). The phosphopantetheine transferase from *Bacillus subtilis* (*Bs*Sfp) was cloned into pCDFDuet-1 plasmid for coexpression with CARs. Expression was carried out in LB media with 0.2 mM isopropyl-β-D-thiogalactopyranoside overnight at 16°C. After harvesting by centrifugation, cells were resuspended in 50 mM Hepes-Na buffer (pH 7.0), and cell-free extracts were prepared by sonication on ice followed by centrifugation. His-Trap Ni-nitrilotriacetic acid Fast Flow (FF) columns were used for protein purification, as described previously (*32*). Purified enzymes were stored at −80°C.

Enzyme activity assay and kinetic analysis

One unit (μmol/min) is defined as the amount of CAR that catalyzes the conversion of 1 μmol of carboxylic acid substrate per minute. Assays were conducted in 100 mM Hepes-Na buffer (pH 7.5) at 30°C, with purified CAR (2 to 20 μg), 1 mM ATP, 0.15 mM NADPH, 10 mM $MgCl_2$, and 5 or 10 mM substrate in a total volume of 1 ml. Substrates α,ω-diacids and ω-amino fatty acids were prepared in dimethyl sulfoxide at 0.5 M, while substrates ω-amino fatty acids were prepared in 100 mM Hepes-Na buffer (pH 7.5) at 0.2 M. CAR activity was measured spectrophotometrically using an NADPH oxidation-based assay to monitor the decrease in absorbance at 340 nm. Blank controls without CARs were included for each set of assays. Triplicate experiments were performed using a UV-1800 UV-VIS Spectrophotometer (Shimadzu).

For the determination of K_M and k_{cat}, kinetic experiments were performed in triplicate using a reaction mixture containing a range of variable substrates (0.5 to 100 mM). Initial reaction rates were fit to the Michaelis-Menten equation using nonlinear least squares regression in Origin 8.0.

Biotransformation by purified enzymes

For the biotransformation of AA to 6-ACA, reaction mixtures (0.2 ml) contained 100 mM Hepes-Na buffer (pH 7.5), 100 mM substrate AA, 1 mM NADPH, 20 mM ATP, 120 mM $MgCl_2$, 120 mM glucose, 1 mM pyridoxal phosphate (PLP), 200 mM isopropylamine (IPA), 100 mM $PolyP_6$, 20 μg of *Bm*GDH, 160 μg of PPK12 (*55*), 292 μg of *Mab*CAR3_G418K, and 360 μg of *Sp*TA, at 30°C, 1000 rpm for 6 hours. The pH was adjusted to 7 by adding 1 M NaOH at 2 and 5 hours, respectively.

For the biotransformation of 6-ACA to HMD, reaction mixtures (0.2 ml) contained Hepes-Na buffer (100 mM, pH 7.5), 100 mM substrate 6-ACA, 1 mM NADPH, 20 mM ATP, 120 mM $MgCl_2$, 100 mM $PolyP_6$, 1 mM PLP, 200 mM IPA, 120 mM glucose, 160 μg of PPK12, 40 μg of the *Bm*GDH, 360 μg of *Sp*TA, and 292 μg of *Mab*CAR3_ACA-4 (6 hours, 1000 rpm, 30°C). The pH was adjusted to 7 by adding 1 M NaOH at 2 and 5 hours, respectively.

For the biotransformation of AA to HMD, reaction mixtures (0.2 ml) contained 100 mM Hepes-Na buffer (pH 7.5), 100 mM substrate AA, 2 mM NADPH, 20 mM ATP, 120 mM $MgCl_2$, 200 mM glucose, 1 mM PLP, 400 mM IPA, 200 mM $PolyP_6$, 40 μg of *Bm*GDH, 160 μg of PPK12, 80 μg of *Mab*CAR3_ACA-1, 884 μg of *Mab*CAR3_ACA-4, and 720 μg of *Sp*TA at 30°C, 1000 rpm for 8 hours. The pH was adjusted to 7 by adding 1 M NaOH at 2 and 5 hours, respectively.

Biotransformation by crude enzymes

For the biotransformation of α,ω-diacids to ω-amino fatty acids (C6-C9), reaction mixtures (10 ml) contained 500 mM Hepes-Na buffer (pH 6.5), 100 mM substrate α,ω-diacids (C6-C9), 1 mM $NADP^+$, 10 mM ATP, 120 mM $MgCl_2$, 120 mM glucose, 1 mM PLP, 200 mM IPA, 100 mM $PolyP_6$, lyophilized enzyme powder of *Bm*GDH (5 mg/ml), lyophilized enzyme powder of PPK12 (15 mg/ml), crude cell extract of *Mab*CAR3_G418K (100 mg/ml), crude cell extract of *Sp*TA (120 mg/ml) at 30°C, 800 rpm. The pH was kept constant at 6.5 with the addition of 2 M NaOH using the pH-Stat (Tiamo) instrument.

Furthermore, for the preparative biotransformation experiment (fig. S11), the reaction mixture was scaled up to 400 ml, with the substrate AA concentration reduced to 50 mM.

For the biotransformation of AA to HMD, reaction mixtures (10 ml) contained 500 mM Hepes-Na buffer (pH 7.5), 50 mM substrate AA, 1 mM $NADP^+$, 10 mM ATP, 120 mM $MgCl_2$, 120 mM glucose, 1 mM PLP, 200 mM IPA, 100 mM $PolyP_6$, lyophilized enzyme powder of *Bm*GDH (8 mg/ml), lyophilized enzyme powder of PPK12 (20 mg/ml), crude cell extract of *Mab*CAR3_ACA-1 (50 mg/ml), crude cell extract of *Mab*CAR3_ACA-4 (100 mg/ml), and crude cell extract of *Sp*TA (240 mg/ml) at 30°C, 800 rpm. The pH was kept constant at 7.5 with the addition of 2 M NaOH using the pH-Stat (Tiamo) instrument.

Sample derivatization

To detect aliphatic α,ω-diacids, 6-hydroxyhexanoic acid and 1,6-hexanediol, 100 μl of reaction mixtures was acidified with 2 μl of 6 M HCl to pH below 2.0 and extracted with 1 ml of EtOAc (1000 rpm, 2 min). The organic phase was dried with anhydrous Na_2SO_4 for 12 hours and centrifuged at 10,000*g* for 2 min. Supernatant solutions (50 μl), a mixture of methanol/ether (50 μl, volume ratio of 1:1), and trimethylsilyl-diazomethane (10 μl, 2 M in hexane) were added to new 1.5-ml tubes. The reactant mixture was incubated at room temperature for 20 min and used for gas chromatography analysis.

To determine ω-amino fatty acids, 100 μl of reaction mixtures was adjusted to pH over 12.0 with 2 μl of 6 M NaOH, mixed with 500 μl of acetonitrile, and centrifuged. The supernatant (20 μl) was mixed with 14 mM Marfey reagent in acetonitrile (20 μl), 1 M sodium bicarbonate (36 μl), and dimethylsulfoxide (100 μl) and incubated at 40°C for 1 hour. The reaction was quenched with 40 μl of 1 M HCl solution and used for high-performance liquid chromatography (HPLC) analysis.

To detect α,ω-diamines, 100 μl of reaction mixtures was adjusted to pH over 12.0 with 6 M NaOH, and 42 μl of supernatant sample mixed with 75 μl of saturated sodium bicarbonate, 250 μl of dansyl chloride in acetonitrile (5 g $liter^{-1}$), and 133 μl of Hepes-Na buffer (pH 7.5). The mixture was sonicated for 10 min, followed by standing for 10 min and then adding 500 μl of methanol and used for HPLC analysis.

Analytical methods

The quantification of α,ω-diacids, 6-hydroxyhexanoic acid and 1,6-hexanediol, were carried out using a Shimadzu GC-2030 system equipped with a flame ionization detector and SH-Rtx-5Sil MS column (30 m by 0.25 mm, 0.25 μm) (fig. S13). The injector and detector temperatures were 250° and 280°C, respectively. The temperature program was held at 85°C for 3 min, increased by 5°C per min to

100°C, further increased by 15°C per min to 250°C, and held at 250°C for 2 min.

The analysis of ω-amino fatty acids and α,ω-diamines was performed using a Shimadzu LC-2014 system with an Elite Hypersil ODS2 column (250 mm by 4.6 mm, 5 μm). ω-amino fatty acids and α,ω-diamines were eluted with methanol/water (1 ml/min; 0.1% trifluoroacetic acid) in a 50:50 ratio and 83:17 ratio, respectively (fig. S13). The autosampler temperature was maintained at 35°C, and the injection volume was 10 μl. The detection wavelengths for ω-amino fatty acids and α,ω-diamines were 340 and 254 nm, respectively.

Statistical analysis

Data were collected from three independent biological replicates, and mean values with SE were calculated. Statistical analysis was performed using Origin 8.0, and one-way analysis of variance (ANOVA) with *t* test was used to determine significant differences. $P < 0.05$ was considered significantly different.

Supplementary Materials

This PDF file includes:

Figs. S1 to S13

Tables S1 to S7

REFERENCES AND NOTES

1. R. D. Süssmuth, A. Mainz, Nonribosomal peptide synthesis—principles and prospects. *Angew. Chem. Int. Ed. Engl.* **56**, 3770–3821 (2017).
2. J. M. Reimer, M. Eivaskhani, I. Harb, A. Guarné, M. Weigt, T. M. Schmeing, Structures of a dimodular nonribosomal peptide synthetase reveal conformational flexibility. *Science* **366**, eaaw4388 (2019).
3. K. D. Patel, M. R. MacDonald, S. F. Ahmed, J. Singh, A. M. Gulick, Structural advances toward understanding the catalytic activity and conformational dynamics of modular nonribosomal peptide synthetases. *Nat. Prod. Rep.* **40**, 1550–1582 (2023).
4. M. Alanjary, C. Cano-Prieto, H. Gross, M. H. Medema, Computer-aided re-engineering of nonribosomal peptide and polyketide biosynthetic assembly lines. *Nat. Prod. Rep.* **36**, 1249–1261 (2019).
5. K. A. J. Bozhüyük, F. Fleischhacker, A. Linck, F. Wesche, A. Tietze, C.-P. Niesert, H. B. Bode, De novo design and engineering of non-ribosomal peptide synthetases. *Nat. Chem.* **10**, 275–281 (2018).
6. D. L. Niquille, D. A. Hansen, T. Mori, D. Fercher, H. Kries, D. Hilvert, Nonribosomal biosynthesis of backbone-modified peptides. *Nat. Chem.* **10**, 282–287 (2018).
7. K. A. J. Bozhüyük, A. Linck, A. Tietze, J. Kranz, F. Wesche, S. Nowak, F. Fleischhacker, Y.-N. Shi, P. Grün, H. B. Bode, Modification and de novo design of non-ribosomal peptide synthetases using specific assembly points within condensation domains. *Nat. Chem.* **11**, 653–661 (2019).
8. K. A. J. Bozhüyük, L. Präve, C. Kegler, L. Schenk, S. Kaiser, C. Schelhas, Y.-N. Shi, W. Kuttenlochner, M. Schreiber, J. Kandler, M. Alanjary, T. M. Mohiuddin, M. Groll, G. K. A. Hochberg, H. B. Bode, Evolution-inspired engineering of nonribosomal peptide synthetases. *Science* **383**, eadg4320 (2024).
9. A. Stanišić, H. Kries, Adenylation domains in nonribosomal peptide engineering. *ChemBioChem* **20**, 1347–1356 (2019).
10. K. A. J. Bozhueyuek, J. Watzel, N. Abbood, H. B. Bode, Synthetic zippers as an enabling tool for engineering of non-ribosomal peptide synthetases**. *Angew. Chem. Int. Ed. Engl.* **60**, 17531–17538 (2021).
11. D. Gahloth, M. S. Dunstan, D. Quaglia, E. Klumbys, M. P. Lockhart-Cairns, A. M. Hill, S. R. Derrington, N. S. Scrutton, N. J. Turner, D. Leys, Structures of carboxylic acid reductase reveal domain dynamics underlying catalysis. *Nat. Chem. Biol.* **13**, 975–981 (2017).
12. W. Finnigan, A. Thomas, H. Cromar, B. Gough, R. Snajdrova, J. P. Adams, J. A. Littlechild, N. J. Harmer, Characterization of carboxylic acid reductases as enzymes in the toolbox for synthetic chemistry. *ChemCatChem* **9**, 1005–1017 (2017).
13. H. Stolterfoht, G. Steinkellner, D. Schwendenwein, T. Pavkov-Keller, K. Gruber, M. Winkler, Identification of key residues for enzymatic carboxylate reduction. *Front. Microbiol.* **9**, 250 (2018).
14. H. Stolterfoht, D. Schwendenwein, C. W. Sensen, F. Rudroff, M. Winkler, Four distinct types of E.C. 1.2.1.30 enzymes can catalyze the reduction of carboxylic acids to aldehydes. *J. Biotech.* **257**, 222–232 (2017).
15. T. P. Fedorchuk, A. N. Khusnutdinova, R. Flick, A. F. Yakunin, Site-directed mutagenesis and stability of the carboxylic acid reductase MAB4714 from *Mycobacterium abscessus*. *J. Biotech.* **303**, 72–79 (2019).
16. M. Baunach, S. Chowdhury, P. Stallforth, E. Dittmann, The landscape of recombination events that create nonribosomal peptide diversity. *Mol. Biol. Evol.* **38**, 2116–2130 (2021).
17. G. Qu, M. Fu, L. Zhao, B. Liu, P. Liu, W. Fan, J.-A. Ma, Z. Sun, Computational Insights into the catalytic mechanism of bacterial carboxylic acid reductase. *J. Chem. Inf. Model.* **59**, 832–841 (2019).
18. Y. Cui, J. Sun, B. Wu, Computational enzyme redesign: Large jumps in function. *Trends Chem.* **4**, 409–419 (2022).
19. C.-Y. Chen, I. Georgiev, A. C. Anderson, B. R. Donald, Computational structure-based redesign of enzyme activity. *Proc. Natl. Acad. Sci. U.S.A.* **106**, 3764–3769 (2009).
20. T. C. Bruice, Computational approaches: Reaction trajectories, structures, and atomic motions. Enzyme reactions and proficiency. *Chem. Rev.* **106**, 3119–3139 (2006).
21. H. J. Wijma, R. J. Floor, S. Bjelic, S. J. Marrink, D. Baker, D. B. Janssen, Enantioselective enzymes by computational design and in silico screening. *Angew. Chem. Int. Ed. Engl.* **54**, 3726–3730 (2015).
22. H. J. Wijma, S. J. Marrink, D. B. Janssen, Computationally efficient and accurate enantioselectivity modeling by clusters of molecular dynamics simulations. *J. Chem. Inf. Model.* **54**, 2079–2092 (2014).
23. Y. Hu, Z. Zhu, D. Gradischnig, M. Winkler, J. Nielsen, V. Siewers, Engineering carboxylic acid reductase for selective synthesis of medium-chain fatty alcohols in yeast. *Proc. Natl. Acad. Sci. U.S.A.* **117**, 22974–22983 (2020).
24. R. Tramontina, J. L. Galman, F. Parmeggiani, S. R. Derrington, T. D. H. Bugg, N. J. Turner, F. M. Squina, N. Dixon, Consolidated production of coniferol and other high-value aromatic alcohols directly from lignocellulosic biomass. *Green Chem.* **22**, 144–152 (2020).
25. S. Henritzi, M. Fischer, M. Grininger, M. Oreb, E. Boles, An engineered fatty acid synthase combined with a carboxylic acid reductase enables de novo production of 1-octanol in *Saccharomyces cerevisiae*. *Biotechnol. Biofuels* **11**, 150 (2018).
26. M. K. Akhtar, N. J. Turner, P. R. Jones, Carboxylic acid reductase is a versatile enzyme for the conversion of fatty acids into fuels and chemical commodities. *Proc. Natl. Acad. Sci. U.S.A.* **110**, 87–92 (2013).
27. C. Lu, E. O. Akwafo, R. H. Wijffels, V. A. P. Martins Dos Santos, R. A. Weusthuis, Metabolic engineering of *Pseudomonas putida* KT2440 for medium-chain-length fatty alcohol and ester production from fatty acids. *Metab. Eng.* **75**, 110–118 (2023).
28. N. D. Butler, S. R. Anderson, R. M. Dickey, P. Nain, A. M. Kunjapur, Combinatorial gene inactivation of aldehyde dehydrogenases mitigates aldehyde oxidation catalyzed by *E. coli* resting cells. *Metab. Eng.* **77**, 294–305 (2023).
29. X. Cen, Y. Liu, F. Zhu, D. Liu, Z. Chen, Metabolic engineering of *Escherichia coli* for high production of 1,5-pentanediol via a cadaverine-derived pathway. *Metab. Eng.* **74**, 168–177 (2022).
30. M. Wang, H. Zhao, Characterization and engineering of the adenylation domain of a NRPS-like protein: A potential biocatalyst for aldehyde generation. *ACS Catal.* **4**, 1219–1225 (2014).
31. N. Butler, A. M. Kunjapur, Carboxylic acid reductases in metabolic engineering. *J. Biotech.* **307**, 1–14 (2020).
32. K. Shi, J.-M. Li, Z.-J. Zhang, Q. Chen, J.-H. Xu, H.-L. Yu, Virtual screening of carboxylic acid reductases for biocatalytic synthesis of 6-aminocaproic acid and 1,6-hexamethylenediamine. *Biotechnol. Bioeng.* **120**, 1773–1783 (2023).
33. T. P. Fedorchuk, A. N. Khusnutdinova, E. Evdokimova, R. Flick, R. Di Leo, P. Stogios, A. Savchenko, A. F. Yakunin, One-pot biocatalytic transformation of adipic acid to 6-aminocaproic acid and 1,6-hexamethylenediamine using carboxylic acid reductases and transaminases. *J. Am. Chem. Soc.* **142**, 1038–1048 (2020).
34. L. Kramer, X. Le, M. Rodriguez, M. A. Wilson, J. Guo, W. Niu, Engineering carboxylic acid reductase (CAR) through a whole-cell growth-coupled NADPH recycling strategy. *ACS Synth. Biol.* **9**, 1632–1637 (2020).
35. D. Schwendenwein, A. K. Ressmann, M. Doerr, M. Höhne, U. T. Bornscheuer, M. D. Mihovilovic, F. Rudroff, M. Winkler, Random mutagenesis-driven improvement of carboxylate reductase activity using an amino benzamidoxime-mediated high-throughput assay. *Adv. Synth. Catal.* **361**, 2544–2549 (2019).
36. E. Marcos, M. J. Field, R. Crehuet, Pentacoordinated phosphorus revisited by high-level QM/MM calculations. *Proteins* **78**, 2405–2411 (2010).
37. M. Zemmouche, C. García-Iriepa, I. Navizet, Light emission colour modulation study of oxyluciferin synthetic analogues via QM and QM/MM approaches. *Phys. Chem. Chem. Phys.* **22**, 82–91 (2020).
38. T. Rungrotmongkol, A. J. Mulholland, S. Hannongbua, Active site dynamics and combined quantum mechanics/molecular mechanics (QM/MM) modelling of a HIV-1 reverse transcriptase/DNA/dTTP complex. *J. Mol. Graph. Model.* **26**, 1–13 (2007).
39. S. Dutta, A. Chandra, Free energy landscape of the adenylation reaction of the aminoacylation process at the active site of aspartyl tRNA synthetase. *J. Phys. Chem. B* **126**, 5821–5831 (2022).

40. M. G. Khrenova, A. M. Kulakova, A. V. Nemukhin, Light-induced change of arginine conformation modulates the rate of adenosine triphosphate to cyclic adenosine monophosphate conversion in the optogenetic System containing photoactivated adenylyl cyclase. *J. Chem. Inf. Model.* **61**, 1215–1225 (2021).
41. W. B. Black, L. Zhang, W. S. Mak, S. Maxel, Y. Cui, E. King, B. Fong, A. Sanchez Martinez, J. B. Siegel, H. Li, Engineering a nicotinamide mononucleotide redox cofactor system for biocatalysis. *Nat. Chem. Biol.* **16**, 87–94 (2020).
42. W. Zheng, Z. Pu, L. Xiao, G. Xu, L. Yang, H. Yu, J. Wu, Mutability-landscape-guided engineering of L -threonine aldolase revealing the prelog rule in mediating diastereoselectivity of C—C Bond formation. *Angew. Chem. Int. Ed. Engl.* **62**, e202213855 (2023).
43. J.-Y. van der Meer, L. Biewenga, G. J. Poelarends, The generation and exploitation of protein mutability landscapes for enzyme engineering. *ChemBioChem* **17**, 1792–1799 (2016).
44. A. N. Khusnutdinova, R. Flick, A. Popovic, G. Brown, A. Tchigvintsev, B. Nocek, K. Correia, J. C. Joo, R. Mahadevan, A. F. Yakunin, Exploring bacterial carboxylate reductases for the reduction of bifunctional carboxylic acids. *Biotechnol. J.* **12**, 1600751 (2017).
45. M. Zhao, D. Huang, X. Zhang, M. A. G. Koffas, J. Zhou, Y. Deng, Metabolic engineering of *Escherichia coli* for producing adipic acid through the reverse adipate-degradation pathway. *Metab. Eng.* **47**, 254–262 (2018).
46. J. Citoler, S. R. Derrington, J. L. Galman, H. Bevinakatti, N. J. Turner, A biocatalytic cascade for the conversion of fatty acids to fatty amines. *Green Chem.* **21**, 4932–4935 (2019).
47. J.-M. Li, K. Shi, A.-T. Li, Z.-J. Zhang, H.-L. Yu, J.-H. Xu, Development of a thermodynamically favorable multi-enzyme cascade reaction for efficient sustainable production of ω-amino fatty acids and α,ω-diamines. *ChemSusChem* **17**, e202301477 (2023).
48. C. Bissantz, B. Kuhn, M. Stahl, A Medicinal chemist's guide to molecular interactions. *J. Med. Chem.* **53**, 5061–5084 (2010).
49. L. Yang, K. Zhang, M. Xu, Y. Xie, X. Meng, H. Wang, D. Wei, Mechanism-guided computational design of ω-transaminase by reprograming of High-energy-barrier steps. *Angew. Chem. Int. Ed. Engl.* **61**, e202212555 (2022).
50. Q. Meng, C. Ramírez-Palacios, N. Capra, M. E. Hooghwinkel, S. Thallmair, H. J. Rozeboom, A.-M. W. H. Thunnissen, H. J. Wijma, S. J. Marrink, D. B. Janssen, Computational redesign of an ω-transaminase from *Pseudomonas jessenii* for asymmetric synthesis of enantiopure bulky amines. *ACS Catal.* **11**, 10733–10747 (2021).
51. Y. Ren, Z. Qin, C. Li, B. Yuan, Y. Yang, G. Qu, Z. Sun, Engineering the activity and thermostability of a carboxylic acid reductase in the conversion of vanillic acid to vanillin. *J. Biotech.* **386**, 19–27 (2024).
52. G. Qu, B. Liu, K. Zhang, Y. Jiang, J. Guo, R. Wang, Y. Miao, C. Zhai, Z. Sun, Computer-assisted engineering of the catalytic activity of a carboxylic acid reductase. *J. Biotech.* **306**, 97–104 (2019).
53. J. Jumper, R. Evans, A. Pritzel, T. Green, M. Figurnov, O. Ronneberger, K. Tunyasuvunakool, R. Bates, A. Žídek, A. Potapenko, A. Bridgland, C. Meyer, S. A. A. Kohl, A. J. Ballard, A. Cowie, B. Romera-Paredes, S. Nikolov, R. Jain, J. Adler, T. Back, S. Petersen, D. Reiman, E. Clancy, M. Zielinski, M. Steinegger, M. Pacholska, T. Berghammer, S. Bodenstein, D. Silver, O. Vinyals, A. W. Senior, K. Kavukcuoglu, P. Kohli, D. Hassabis, Highly accurate protein structure prediction with AlphaFold. *Nature* **596**, 583–589 (2021).
54. N. G. Bozhanova, J. M. Harp, B. J. Bender, A. S. Gavrikov, D. A. Gorbachev, M. S. Baranov, C. B. Mercado, X. Zhang, K. A. Lukyanov, A. S. Mishin, J. Meiler, Computational redesign of a fluorogen activating protein with Rosetta. *PLOS Comput. Biol.* **17**, e1009555 (2021).
55. M. Tavanti, J. Hosford, R. C. Lloyd, M. J. B. Brown, ATP regeneration by a single polyphosphate kinase powers multigram-scale aldehyde synthesis in vitro. *Green Chem.* **23**, 828–837 (2021).
56. Z. Zhang, L. Fang, F. Wang, Y. Deng, Z. Jiang, A. Li, Transforming inert cycloalkanes into α,ω-diamines by designed enzymatic cascade catalysis. *Angew. Chem. Int. Ed. Engl.* **62**, e202215935 (2023).
57. S. Sarak, A. D. Pagar, T. P. Khobragade, H. Jeon, P. Giri, S. Lim, M. D. Patil, Y. Kim, B.-G. Kim, H. Yun, A multienzyme biocatalytic cascade as a route towards the synthesis of α,ω-diamines from corresponding cycloalkanols. *Green Chem.* **25**, 543–549 (2023).
58. L. Wang, G. Li, A. Li, Y. Deng, Directed synthesis of biobased 1,6-diaminohexane from adipic acid by rational regulation of a functional enzyme cascade in *Escherichia coli*. *ACS Sustain. Chem. Eng.* **11**, 6011–6020 (2023).
59. S. Sarak, T. P. Khobragade, H. Jeon, A. D. Pagar, P. Giri, S. Lee, H. Yun, One-pot biocatalytic synthesis of nylon monomers from cyclohexanol using *Escherichia coli* -based concurrent cascade consortia. *Green Chem.* **23**, 9447–9453 (2021).
60. S. Sarak, S. Sung, H. Jeon, M. D. Patil, T. P. Khobragade, A. D. Pagar, P. E. Dawson, H. Yun, An integrated cofactor/co-product recycling cascade for the biosynthesis of nylon monomers from cycloalkylamines. *Angew. Chem. Int. Ed. Engl.* **60**, 3481–3486 (2021).
61. L. Bretschneider, M. Wegner, K. Bühler, B. Bühler, R. Karande, One-pot synthesis of 6-aminohexanoic acid from cyclohexane using mixed-species cultures. *Microb. Biotechnol.* **14**, 1011–1025 (2021).
62. S. C. H. J. Turk, W. P. Kloosterman, D. K. Ninaber, K. P. A. M. Kolen, J. Knutova, E. Suir, M. Schürmann, P. C. Raemakers-Franken, M. Müller, S. M. A. De Wildeman, L. M. Raamsdonk, R. Van Der Pol, L. Wu, M. F. Temudo, R. A. M. Van Der Hoeven, M. Akeroyd, R. E. Van Der Stoel, H. J. Noorman, R. A. L. Bovenberg, A. C. Trefzer, Metabolic engineering toward sustainable production of Nylon-6. *ACS Synth. Biol.* **5**, 65–73 (2016).

Acknowledgments: We would like to thank W. S. Mak and B. Wu for useful discussions. **Funding:** This work was supported by the National Key Research and Development Program of China 2019YFA0905000 (to H.-L.Y.) and 2021YFC2102900 (to H.-L.Y.), the Shanghai Commission of Science and Technology 23HC1400200 (to H.-L.Y.), the National Natural Science Foundation of China 32401276 (to K.S.) , 21922804 (to H.-L.Y.), and 32271540 (to H.-L.Y.), the Program of Shanghai Academic Research Leader 21XD1400800 (to H.-L.Y.), and the Frontiers Science Center for Materiobiology and Dynamic Chemistry JKVF12001035 (to J.-H.X.). **Author contributions:** K.S. and H.-L.Y. initiated the project. K.S. and M.-Q.W. performed the computational work. K.S., J.-M.L., and Y.-K.Z. performed biocatalytic experiments. K.S., J.-M.L, H.-L.Y., Z.-J.Z., Q.C., F.H., and J.-H.X. provided supervision and input on experimental design. K.S. wrote the manuscript, which was revised and approved by all authors. **Competing interests:** Three patents are currently pending, filed by the East China University of Science and Technology. The authors K.S., J.-M.L., Z.-J.Z., and H.-L.Y., who contributed to this paper, are also listed as inventors on these patents. The first patent, filed on 9 January 2023, is currently pending under the serial number CN116179500A. The second patent, filed on 15 September 2023, is currently pending under the serial number CN117343971A. The third patent, filed on 27 March 2024, is currently pending under the serial number PCT/CN2024/084036. All authors declare that they have no other competing interests. **Data and materials availability:** All data needed to evaluate the conclusions in the paper are present in the paper and/or the Supplementary materials. Bacterial strains and recombinant plasmids used in this work are provided by East China University of Science and Technology pending scientific review and a completed material transfer agreement. Requests for these strains and plasmids should be submitted to H.-L.Y. (huileiyu@ecust.edu.cn).

Submitted 26 May 2024
Accepted 25 October 2024
Published 29 November 2024
10.1126/sciadv.adp6775